Published online 2 November 2015 *Nucleic Acids Research, 2015, Vol. 43, No. 22* ***10861–10869***
doi: 10.1093/nar/gkv1150

Allosteric ring assembly and chemo-mechanical melting by the interaction between 5′-phosphate and λ exonuclease

Jungmin Yoo and Gwangrog Lee*

School of life Sciences, Gwangju Institute of Science and Technology, Gwangju 500-712, Korea

Received September 23, 2015; Revised October 19, 2015; Accepted October 19, 2015

ABSTRACT

Phosphates along the DNA function as chemical energy frequently used by nucleases to drive their enzymatic reactions. Exonuclease functions as a machine that converts chemical energy of the phosphodiester-chain into mechanical work. However, the roles of phosphates during exonuclease activities are unknown. We employed λ exonuclease as a model system and investigated the roles of phosphates during degradation via single-molecule fluorescence resonance energy transfer (FRET). We found that 5′ phosphates, generated at each cleavage step of the reaction, chemo-mechanically facilitate the subsequent post-cleavage melting of the terminal base pairs. Degradation of DNA with a nick requires backtracking and thermal fraying at the cleavage site for re-initiation via the formation of a catalytically active complex. Unexpectedly, we discovered that a phosphate of a 5′ recessed DNA acts as a hotspot for an allosteric trimeric-ring assembly without passing through the central channel. Our study provides new insight into the versatile roles of phosphates during the processive enzymatic reaction.

INTRODUCTION

DNA exonucleases are involved in many fundamental genetic processes, such as replication, repair and recombination (1). These enzymes catalyze the excision of nucleosides from 3′- or 5′-termini of nucleic acid substrates. In the case of bacteriophage λ, recombination occurs during infection via the red recombination system by λ exonuclease and an annealing protein (also named Red α and β, respectively) (2,3). λ exonuclease processes an early double stranded(ds) DNA intermediate for homologous recombination. The 3′ single stranded(ss)-overhang generated by λ exonuclease becomes a substrate for the annealing factor of Red β, the activity of which promotes a pairing reaction to initiate homologous recombination with or without the help of host proteins, such as RecA and SSB (4).

DNA is made by connecting the 5′ phosphate (P) and the 3′ hydroxyl (OH) via phosphodiester bonds, and many nucleases recognize 5′ phosphates and hydrolyze phosphodiester bonds. Phosphates along the DNA thus serve as chemical energy for nucleases to drive enzymatic reactions. For example, λ exonuclease functions as a machine that converts chemical energy released from hydrolysis of the phosphodiester-chain into mechanical work to perform the translocation for processive degradation. The processive reaction requires the melting to degrade the dsDNA substrate. Many intriguing questions arise as to how λ exonuclease coordinates its processive translocation activity with the duplex melting, which often acts as a large energy barrier along the reaction-coordinate. First, does λ exonuclease simultaneously melt a single base pair (bp) of duplex DNA every time it cleaves a single nucleotide, as proposed in an ribonuclease system (5)? Alternatively, does λ exonuclease open several base pairs in a burst and degrade one nucleotide at a time, as proposed in other helicase and nuclease systems (6,7). A recent structural study suggested an electrostatic ratchet mechanism for processivity. However, the chemo-mechanical coupling between phosphate hydrolysis and enzymatic actions has not been investigated, and the roles of phosphates during the multiple step enzymatic reaction are also unknown.

Recent advance in single molecule techniques allows us to probe physiologically important dynamic behaviours such as enzymatic heterogeneity (8–10), structure-function relationship (11,12), hidden complexity (1,13,14), and slippage events (15). Previous single molecule studies have revealed that λ exonuclease undergoes a sequence-dependent pausing (16) and dynamic disorder (10). In this study, we employed a single molecule FRET to investigate: (i) how the hydrolytic reaction of 5′ phosphates by λ exonuclease is transduced to mechanical action (melting mechanism); (ii) how the closed ring shape of λ exonuclease is loaded onto various DNA substrates (ring assembly mechanism). We found that the chemo-mechanical melting is achieved by electrostatic attraction of phosphates to the positively

*To whom correspondence should be addressed. Tel: +82 62 715 3558; Fax: +82 62 715 2484; Email: glee@gist.ac.kr

charged pocket at the active site, and discovered that the enzyme allosterically assembles trimeric-ring at a phosphate of 5′-recessed DNA without passing through the central channel. Our study provides new insight into the versatile roles of phosphates during the processive enzymatic reaction.

MATERIALS AND METHODS

Protein purification

The λ exonuclease gene was amplified by PCR from genomic λ phage DNA (D3654-5UN, Sigma Aldrich) using primers designed for ligation-independent cloning (LIC). The PCR product was cloned into the pB4 ($(his)_6$-tag-Maltose Binding Protein (MBP)-TEV site) vector via the LIC method (17). The cloned vector was confirmed by DNA sequencing, and λ exonuclease was expressed in *E. coli* cells. The fusion plasmid construct was transformed into BL21-Star *E. coli* and expressed in 1 L of LB. Bacterial cultures were grown to an OD_{600} of 0.4. Then, IPTG was added at a final concentration of 0.5 mM. After shaking for 3.0 h at 37°C, bacteria were harvested in a rotor at 5000 ×*g* and lysed by sonication in a buffer (50mM Tris–HCl (pH 8.0) and 300 mM NaCl). The cell lysate was centrifuged for 30 min at 35 000 ×*g,* and re-suspended in 50 mM Tris–HCl (pH 8.0), 300 mM NaCl and 10 mM imidazole. λ exonuclease was purified by HisTrap FF (GE Healthcare) using a buffer (50 mM Tris–HCl (pH8.0), 300 mM NaCl and 300 mM Imidazol in a gradient method. $(His)_6$-tag-MBP was removed by TEV protease, which remained five glycines at the N-terminus of the protein, and purified again by HisTrap FF (GE Healthcare). The dialysis was done in 20 mM Tris–HCl (pH 8.0). The purified protein was stored in a buffer (25 mM Tris–HCl (pH 8.0), 50 mM NaCl, 1 mM DTT, 0.1 mM EDTA and 50% glycerol).

Cy3 and Cy5 labeling and annealing

DNA oligonucleotides were purchased from Integrated DNA Technologies (IDT). Two amine-modified oligonucleotides were labeled with Cy3 and Cy5, and the non-hydrolyzed strand was constructed by conjugating both oligos using T4 ligase at room temperature for 3 h. The ligated strand was purified from unreacted oligonucleotides via 15% PAGE gel. The fluorescently labeled non-hydrolyzed DNA was annealed with the 5′ hydrolyzed strand in Tris buffer (pH 8.0) with 100 mM NaCl by heating for 2 min at 85°C and cooling down slowly to room temperature.

Single-molecule FRET assays

Single-molecule experiments were performed with a prism-type total internal reflection fluorescence microscopy. The fluorescence emission light from Cy3 and Cy5 fluorophores was collected by a water-immersion objective lens (UPlanApo 60×, Olympus) and then transmitted through a 550-nm long-pass filter to block a scattered light from a 532 laser. The fluorescence emission spectrum was further separated into donor (green) and acceptor (red) signals with a dichroic mirror with a 630-nm cutoff (Chroma) and detected by back-illuminated electron-multiplying charge-coupled device (897 EMCCD, Andor) with a 100-ms time resolution. Fluorescence signals of donor and acceptor were extracted from the EMCCD camera and amplified by a gain function. Fluorescence areas of both Cy3 and Cy5 were selected by a Gaussian fit and a signal cutoff above the average of the background signals. Single molecule intensities were extracted from the recorded video file by a mapping algorithm compiled in IDL software, and FRET efficiency was calculated as the ratio of intensities (intensity acceptor/(intensity donor + intensity acceptor)) after cross-talk was corrected between the donor and acceptor channels. All the data were analyzed with analysis codes written in MATLAB and plotted in Origin. Single molecule FRET assays were conducted as described previously (18). The reaction buffer for single molecule assays contained 67 mM glycine–KOH (pH 9.4), 3 mM $MgCl_2$, 100 μg ml^{-1} BSA, 1 mg ml^{-1} Trolox, and oxygen-scavenging system of 1 mg ml^{-1} and 0.4 (w/v) D-glucose (Sigma-Aldrich).

Gel-based degradation assay

The 5′ degradation strand of various substrates was fluorescently labeled via 3′ amino-modification with a Cy3 mono NHS ester (GE Healthcare Life Sciences). Substrates for the gel assay were prepared as described in 'Cy3 and Cy5 labeling and annealing'. For a degradation reaction, ∼3–5 pmol of various substrates was mixed with ∼24 pmol λ exonuclease in 50 μl buffer containing 67 mM glycine–KOH (pH 9.4), 3 mM $MgCl_2$, 0.5% glycerol and 100 μg ml^{-1} BSA. The sample was incubated for different time periods at room temperature, and the reactions were quenched by the addition of 50 μl of formamide. The result was resolved on a 15% native PAGE gel for Supplementary Figure S9 and imaged by a fluorescence imager (Typhoon FLA 7000 from GE Healthcare Life Science).

RESULTS

Single-molecule fluorescence assay for λ exonuclease

λ exonuclease forms a ring-shaped homotrimeric structure with a tapered central channel (Figure 1A). This enzyme digests one strand of linear double-stranded (ds)DNA in the 5′ to 3′ direction and generates a 3′ ss-overhang of the non-hydrolyzed strand, releasing 5′ mononucleotides as products. The 3′ overhang produced passes through the ring structure to exit the back of the central channel (Figure 1B). Topological linkage of the ssDNA to the enzyme is attributed to its high processivity (>3000 nucleotides (nt) per attempts), and the tapered structure serves as a converting-platform where dsDNA enters but only ssDNA emerges after degradation. Based on a recent enzyme-substrate structure (19), it was suggested that two nucleotides of the 5′ end strand must be melted and located at the active site of the enzyme prior to degradation by forming a 'catalytically active DNA–protein complex' (Figure 1A, the two nucleotides are noted in violet; and Supplementary Figure S1a). The enzymatic activity is Mg^{2+} and Mn^{2+} dependent but not Ca^{2+} dependent. The catalytic reaction occurs at the active site, which contains a PD-(D/E)XK motif that holds two acidic residues to coordinate two Mg^{2+} ions typically observed in

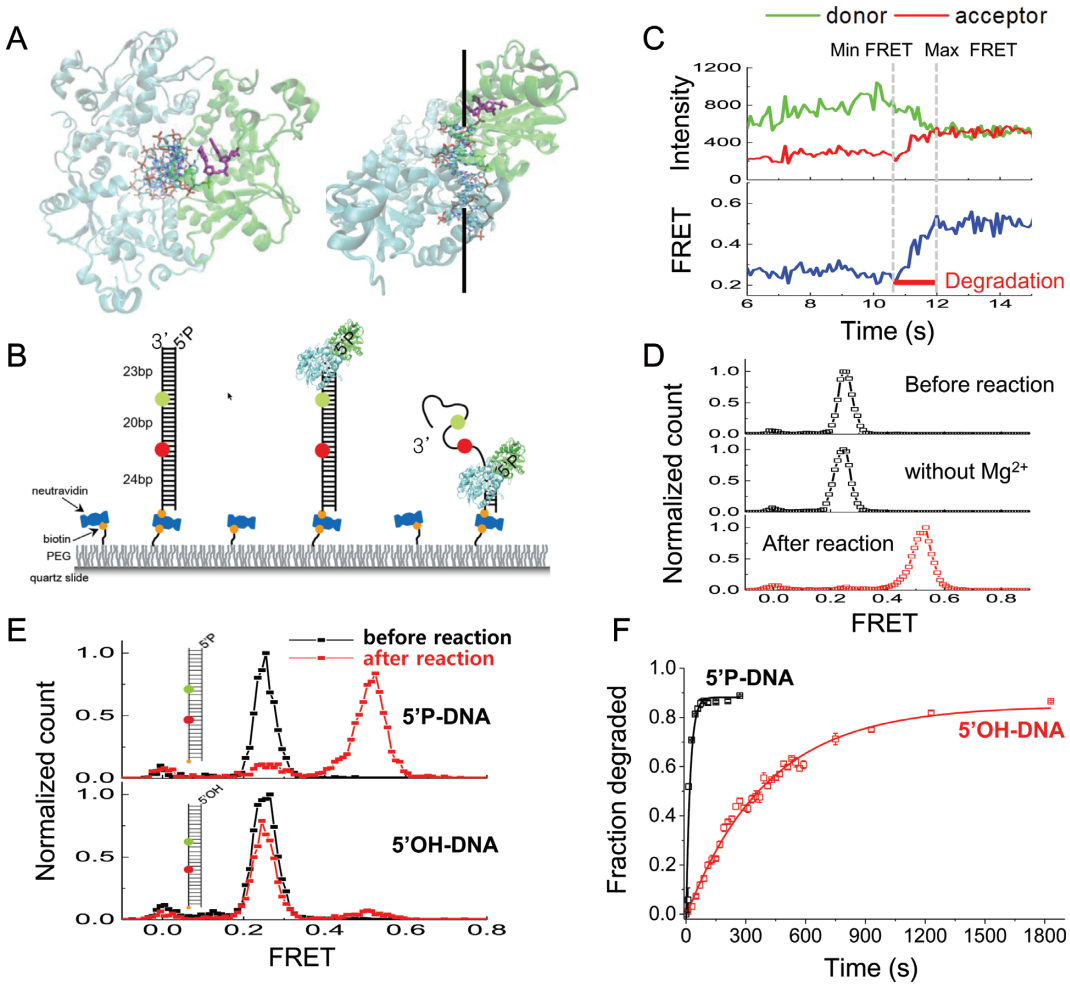

Figure 1. Single molecule FRET assay for DNA degradation. (**A**) Top and side views of the crystal structure of λ exonuclease with DNA (PDB entry 3SM4) demonstrating that two nucleotides (violet) of the 5′-end strand are pre-melted at the ss-ds junction and inserted into the active site of one subunit. (**B**) Experimental scheme, depicting the DNA and protein tilted with an angle relative to the DNA. (**C**) FRET-time trace, demonstrating how degradation time is assigned. (**D**) FRET-histogram that was obtained as shown in (B) (top: dsDNA; middle: before the degradation without Mg^{2+}; bottom: after the degradation with Mg^{2+}). (**E**) FRET-histograms obtained before (black curve) and after (red curve) a 2-min reaction with DNA substrates with (top) and without (bottom) a 5′ terminal phosphate. (**F**) The 5′ terminal phosphate is essential for the formation of a catalytically active DNA and enzyme complex. The fitted exponential growth of 5′P-DNA (black line) and 5′OH-DNA (red line) are 20 s and 403 s, respectively. Error bars denote SEM.

a two-metal mechanism as well as a lysine that activates the hydrolytic water molecule for nucleophilic attack on the scissile phosphate (Supplementary Figure S1a).

We constructed a blunt-ended dsDNA substrate with a 5′ phosphate group on the hydrolyzed strand (Figure 1B). The FRET donor (Cy3) and the acceptor (Cy5) were placed 23 and 43 bp, respectively, into the duplex on the non-hydrolyzed strand. To monitor the processive activity of λ exonuclease in real time at a single-molecule resolution, the DNA substrate was immobilized by a biotin-streptavidin interaction on a polymer-coated quartz surface (Figure 1B). Upon addition of the enzyme and Mg^{2+} to the DNA on the surface, the enzyme converted the rigid dsDNA to ssDNA, degrading the 5′ hydrolyzed strand. The degradation reaction resulted in a FRET increase caused by the decrease in the time-averaged distance between the two fluorophores, but such a time-averaging FRET change did not appear in the absence of Mg^{2+} (Figure 1D). The FRET histogram changed from a peak at E = 0.26 before the reaction to a peak at $E = 0.54$ after the reaction (Figure 1C and D). The complete shift from low to high FRET indicated efficient degradation of DNA by λ exonuclease. The steep FRET increase without intermediate steps indicated that λ exonuclease is indeed processive, as reported in our previous study (18). We measured the degradation time of the labeled 20-nt region over which FRET increased from the minimum to the maximum values (Figure 1C). The degradation rates were calculated by the number of nucleotides (20 nt) divided by the degradation time (1.1 s), thus resulting in ∼18 nt s^{-1}. The processive degradation rates have been measured as 10–12 nt s^{-1} by bulk biochemical studies (20,21) and 13–18 nt s^{-1} by single molecule studies (10,16,18). Our previous study demonstrated that the labeling with iCy3 on DNA substrates had a minimal effect on the degradation (18).

5′OH at the end of dsDNA inhibits a catalytically active complex

A previous biochemical study demonstrated the functional role of the 5′ terminal phosphate in linear dsDNA, where its recognition is essential for efficient degradation of DNA. In addition, the reduced hydrolysis rate of a 5′OH substrate by the enzyme is due to a catalytic defect which causes inert complexes during the initiation of degradation (21). We performed a single-molecule degradation assay using two DNA substrates with or without a phosphate group at the 5′ end of the hydrolyzed strand (termed 5′P-DNA and 5′OH-DNA, respectively). A histogram of 5′P-DNA obtained 2 min after the start of the reaction exhibited complete degradation (Figure 1E, upper panel), whereas the 5′OH-DNA histogram displayed a significantly delay (Figure 1E, lower panel). Because of slow assembly process at low protein concentrations, we measured relative degradation rate via fitting the inverse of characteristic growth time for degradation population with a single exponential growth function. The characteristic degradation times determined (T_d) were ∼20 s for the 5′P-DNA and ∼403 s for the 5′OH-DNA (Figure 1F; see Supplementary Figures S2 and S3 for their distributions). The 20-fold delay for the degradation time in the absence of the 5′ phosphate was qualitatively consistent with the previous finding that catalytically inactive complexes due to catalytic defects were temporarily formed in the absence of the 5′ phosphate (20,21). Indeed, the comparison of real-time FRET trajectories between 5′P-DNA and 5′OH-DNA revealed that the 20-fold delay was mainly due to a longer lag time occurring during initiation (Supplementary Figure S4).

A structural study has proposed that the enzyme utilizes an electrostatic ratchet mechanism for its processive degradation in which the enzymatic translocation along DNA is powered by attraction of the 5′ phosphate terminal group to a positively charged pocket located at the end of the active site (19). We examined how hydrolysis of 5′ phosphates influences the enzymatic activity of λ exonuclease, using a nick as a hydrolysis defect. We introduced a nick with a 5′ phosphate at the fifth position in the 20-bp region of the original substrate between two fluorophores termed nick-5′P-DNA (Figure 2A, second substrate) and compared their degradation pattern with that of intact 5′P-DNA (Figure 2A, first substrate). Although both histograms obtained from nick-5′P-DNA and 5′P-DNA after a 2-min reaction exhibited complete degradation (Figure 2B, first and second panels), a representative individual FRET time trajectory of the nick-5′P-DNA (Figure 2A, second substrate) exhibited a delay that is absent in 5′P-DNA (Figure 2C, compare first and second panels). For example, the enzyme exhibited (i) consistent pauses at $E = 0.33$ (Figure 2C, horizontal arrows and see Supplementary Figure S5); (ii) subsequent backtracking upon encountering the nick site (dotted red circle) and (iii) subsequent progression for degradation (Figure 2C, vertical arrows in the second and fourth panels). The percentage of FRET-time traces showing backtracking events for each substrate is 5′P-DNA: 3% (12/356); nick-5′P-DNA: 66% (206/313); nick-5′OH-DNA: N.A.; nick-5′OH-premelted-DNA: 78% (209/269).

The backtracking can be attributed to the fact that the translocation stops at the nick site such that the enzyme may slide away from the ss-/ds-junction by diffusion because no DNA hydrolysis was involved in the backward movement. By random diffusion, the enzyme stochastically re-engaged and restarted degradation (Figure 2C, see red circle). The restart requires not only melting of 2-nt of the 5′ end but also insertion of the 2-nt to the central channel upon stochastic thermal melting of the terminal base pairs at the ss-/ds-junction. The recent co-crystal structure resolved represents the catalytically active complex (Figure 1 and Supplementary Figure S1a) (19).

5′ Phosphate is essential for the enzyme to melt the terminal base pairs at the ss-/ds-junction

Next, we further investigated how the absence of a phosphate affects translocation and melting steps during processive degradation using a nicked DNA that lacks a 5′ phosphate, termed nick-5′OH-DNA (Figure 2A, third substrate). FRET time trajectories obtained from the nick-5′OH-DNA exhibited more frequent back-and-forth movements at the 5′ OH nick site. However, the exonuclease frequently failed to move past the nick, as indicated by numerous increases and decreases in FRET (Figure 2C, third panel and Figure 3B). Only ∼10% (30 out of 288 molecules) of molecules passed the OH-nick site (Figure 2C, third panel) and the remainder of the molecules randomly diffused away from the junction for a long period of time (Figure 3A and B). The association and dissociation constants between the channel of the enzyme and the 5′ OH terminal junction were 0.074 s^{-1} and 0.084 s^{-1}, respectively (Figure 3C). This failure of degradation suggested that the enzyme acting ahead of the 5′ OH-nick could not perform one of enzymatic key steps, such as duplex melting. Therefore, the enzyme was trapped in a catalytically inactive complex, causing degradation arrest (Figure 2B and C, third panels and Figure 3B).

At present, it remains unknown how those enzymatic steps are ordered and how translocation is temporally coordinated with duplex melting of the terminal base pairs. However, the electrostatic attraction is believed to contribute to the melting of the next base pair upon concomitant translocation. From the co-crystal structure of the DNA-λ exonuclease complex (19), it could be postulated that the enzyme may perform translocation-coupled melting, where the highly positive-charged patch, which contains R28 and two Mg^{2+} ions, attracts scissile phosphates at each round of the reaction (Supplementary Figure S1c), resulting in translocation by one nucleotide at a time and concomitant hydrolysis (19,21). This translocation may pull the 5′ hydrolyzed strand along with destabilization by a hydrophobic wedge of L78 against the base pairs, facilitating melting of the next base pair at the ss-/ds-junction (Supplementary Figure S1a, green residue) (19). In the case of the nick-5′OH-DNA (Figure 2C, third panel), the pulling force by the electrostatic attraction cannot be propagated downstream beyond the nick; thus, melting does not occur. The DNA–enzyme complex is potentially trapped in a catalytically inactive intermediate state immediately before the melting step. The Ca^{2+}-bound 5′-OH DNA-enzyme re-

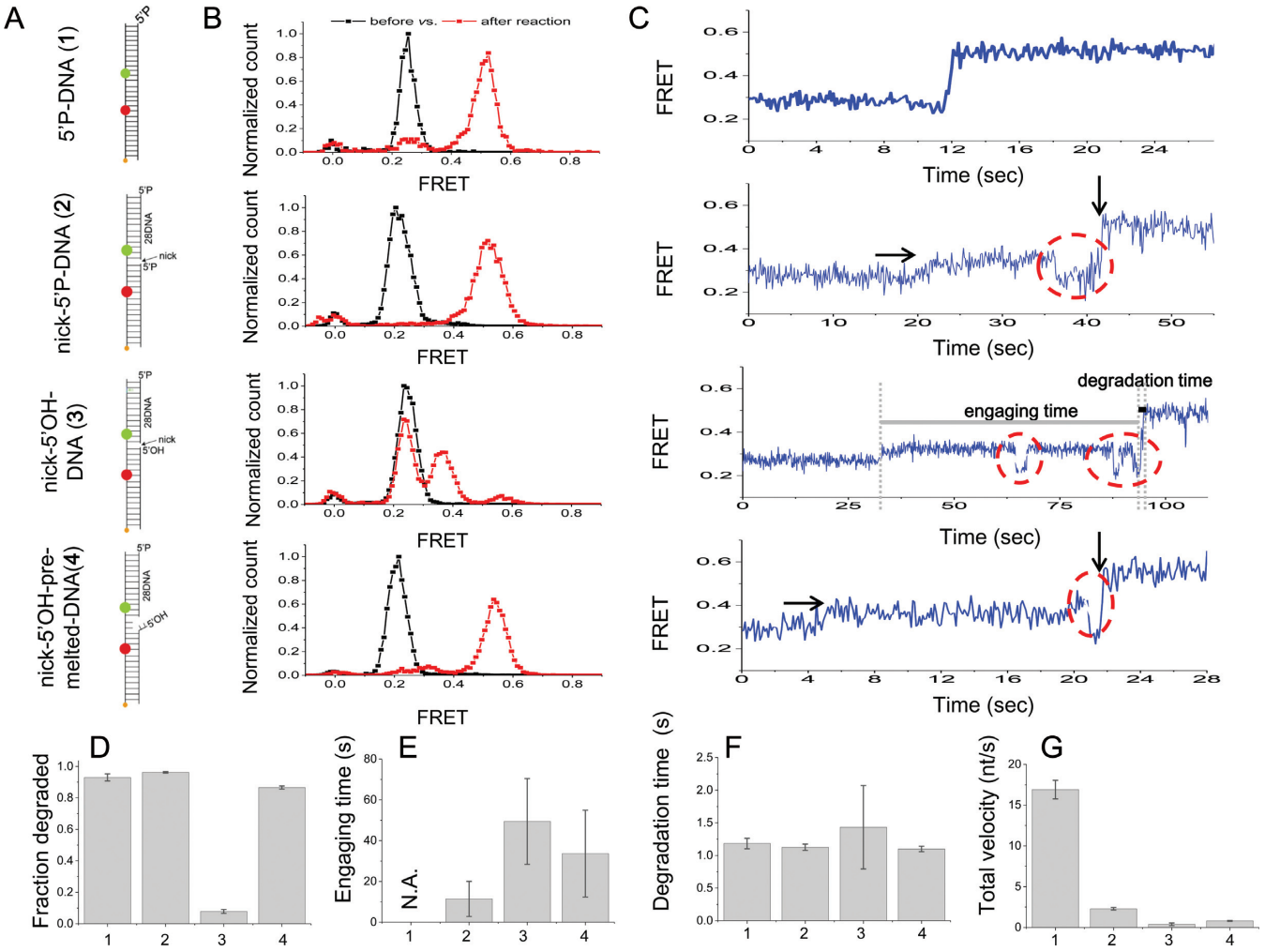

Figure 2. The 5′ phosphate facilitates the melting of terminal base pairs at the ss-/ds-junction, thus guiding the formation of a catalytically active complex. (**A**) Schematics of intact (1), nicked DNA with a phosphate (2), nicked DNA without a phosphate (3), and nicked DNA without a phosphate but pre-melted with two nucleotides (4). (**B**) Histograms obtained before (black curve) and after (red curve) a 2-min reaction for each, corresponding DNA substrate presented in (A). (**C**) FRET time trajectories, depicting pauses (horizontal arrows), backtracking (red circle), and subsequent degradation (vertical arrows). The FRET time trace in the third panel depicts how engaging time and degradation time are assigned. (**D**–**G**) Comparison of degradation of the four DNA substrates presented in (A). (D) Fraction degraded. (E) Engaging time. (F) Degradation time. (G) The inverse of total dwell time. See Supplementary Figures S6–S8 for the distributions. Error bars denote SEM.

solved recently (19) (PDB ID 3SLP, see Supplementary Figure S1b) may represent the inert 5′-OH DNA–enzyme complex we observed, since the 5′ hydrolyzed strands of both the complexes are not plugged into the active site of the enzyme due to the absence of the electrostatic attraction. In this structure, the DNA is partially engaged in the central channel but the 2-nt of the terminal base pairs are not generated and cannot be plugged into the active site (Figure 1A and Supplementary Figure S1b). Presumably, inserting the 5′OH end to the active site was not favorable due to the absence of electrostatic attraction although the thermal opening of 2-nt occurred at the ss-/ds-junction. The 5′ phosphate thus stabilizes the 2 nt ssDNA at the active site of the enzyme for rapid initiation.

5′ pre-melted junction rescues degradation of the nick-5′OH-DNA

To assess whether a 2-nt pre-melted strand of the 5′OH end rescues the degradation arrest, we constructed a nick-5′OH-DNA with a 2-nt mismatched strand at the ss-/ds-junction termed nick-5′OH-pre-melted-DNA (Figure 2A, bottom panel). The degraded fraction was dramatically increased by a factor of 10, from ∼0.08 ± 0.01 (i.e. 8%) for the nicked-5′OH-DNA to 0.86 ± 0.01 (i.e. 86%) for the nicked-5′OH-pre-melted-DNA (Figure 2D, compare 3 and 4). The degradation for the nick-5′OH-premelted DNA reached almost similar levels of degradation obtained from 5′P-DNA and nicked 5′P-DNA (0.93 ± 0.04 and 0.96 ± 0.01, respectively). The rescue by the 2-nt pre-melting DNA structure suggested that interior phosphates not only drive the translocation but also facilitate the melting of the terminal base pairs. To characterize the coupling between the melt-

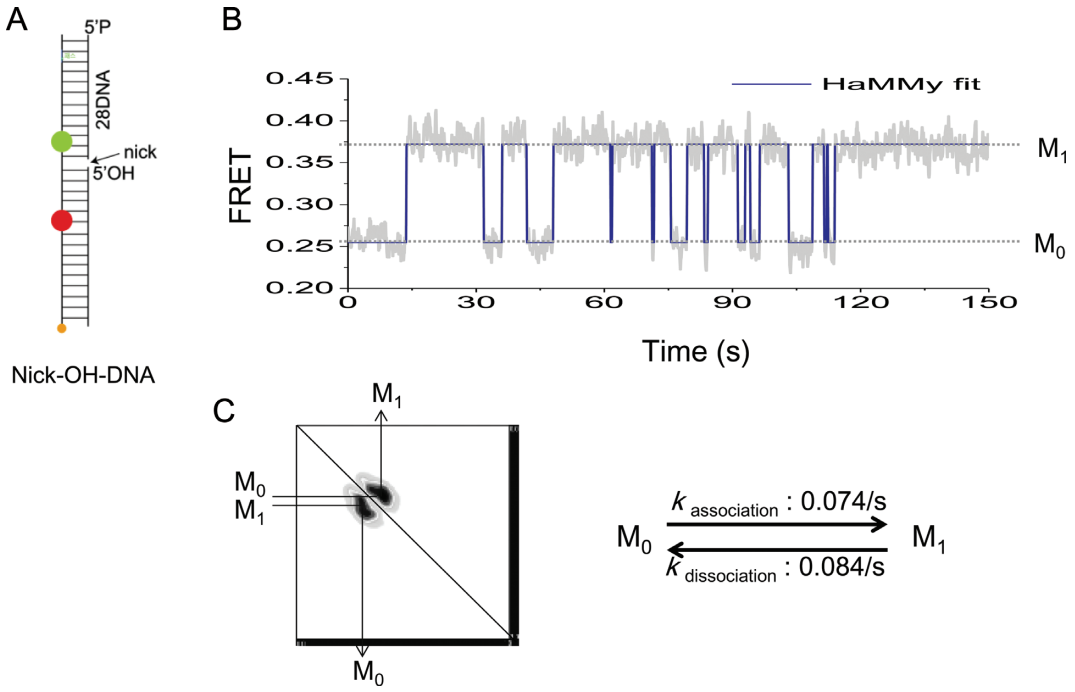

Figure 3. The lack of a phosphate at a nick in the DNA substrate prevents the formation of a stable association with λ exonuclease during degradation. (**A**) Schematic of a DNA substrate without a 5′ phosphate group at a nick in the hydrolyzed strand (nick-5′OH-DNA). (**B**) Exemplary FRET time trajectory demonstrating diffusive back and forth movement of the enzyme in the absence of a 5′ phosphate in the substrate. Approximately 90% of all trajectories exhibited diffusive movements on the nick-5′OH-DNA. The blue trace is an idealized fit that is used to extract association and dissociation rates based on the HaMMy (25) algorithm. (**C**) Transition density plots (TDP) generated from the FRET value before transition (association of the enzyme) on the x-axis and the FRET value after transition (dissociation of the enzyme) on the y-axis. To extract association and dissociation constants, HaMMy (25) analysis was performed based on 161 individual FRET time trajectories.

ing and translocation, we defined two different time periods (Figure 2C, third panel): (i) the 'engaging time' during which the enzyme attempts to proceed past the nick site but often fails and moves backwards due to the absence of the phosphate, as indicated by a drop in FRET; and (ii) the 'degradation time' during which the FRET signal increases from the minimum to the maximum values. We compared engaging and degradation times for all the constructs (Figure 2E and F). The engaging time of the nick-5′OH-premelted-DNA was reduced ∼31%, compared to the nick-5′OH-DNA (Figure 2E; see Supplementary Figures S6–S8 for their distributions). In contrast, the degradation times of all the constructs were similar (Figure 2F). This data supported the notion that the negative-charged phosphate at the nick indeed guides the 5′ terminal 2-nt to the positively charged channel of the enzyme by electrostatic attraction upon thermal melting. The order of the overall degradation rate was P-DNA, nicked 5′P-DNA, nicked 5′OH-premelted-DNA, and nicked 5′OH-DNA (Figure 2G). The order difference comes from the fact that P-DNA is intact; nicked-5′P-DNA has a broken backbone; nicked 5′OH-premelted-DNA has a broken backbone without the 5′ phosphate. But, nicked 5′OH-premelted-DNA partially compensates the effect of the absence of the 5′ phosphate via premelting. The slowing-down effects in engaging time, degradation time and total velocity clearly recapitulate the important role of the 5′ phosphate during the degradation.

5′-Phosphate facilitates allosteric ring assembly without passing through the central channel

The functional form of λ exonuclease is thought to be a stable trimer ring, but this widely held assumption has not been directly demonstrated. The fact that a single protein binding event detected via FRET change was insufficient to catalyze reactions raises a question regarding trimer stability in solution (18). Thus, we asked whether λ exonuclease can re-assemble the ring structure if it dissociates from DNA after producing a long 3′ ss-overhang with thousands of nucleotides, which is its average processivity. The threading of such a long 3′ strand through the trimeric channel is an inefficient method such that the enzyme may utilize an unknown re-initiating mechanism for degradation. In addition, such a long ssDNA has a high probability to form secondary structures so that λ exonuclease may have difficulty in passing through regions of secondary structures (22).

We hypothesized that the enzyme may reassemble the trimeric ring around the ss-/ds-junction. To test this hypothesis, we constructed a series of DNA/RNA hybrids with different ss-gap sizes (Figure 4A). The upstream strand (top) was hybridized with an RNA oligo (Figure 4A, top red strand), thus preventing degradation from the 5′ end of the DNA/RNA hybrid. In contrast, the downstream strand (Figure 4A, bottom black strand) was hybridized with a DNA oligo, allowing degradation from the 5′ end of the gap junction only via a trimeric assembly around the ss-gap between RNA and DNA oligos (Figure 4A). A gel assay con-

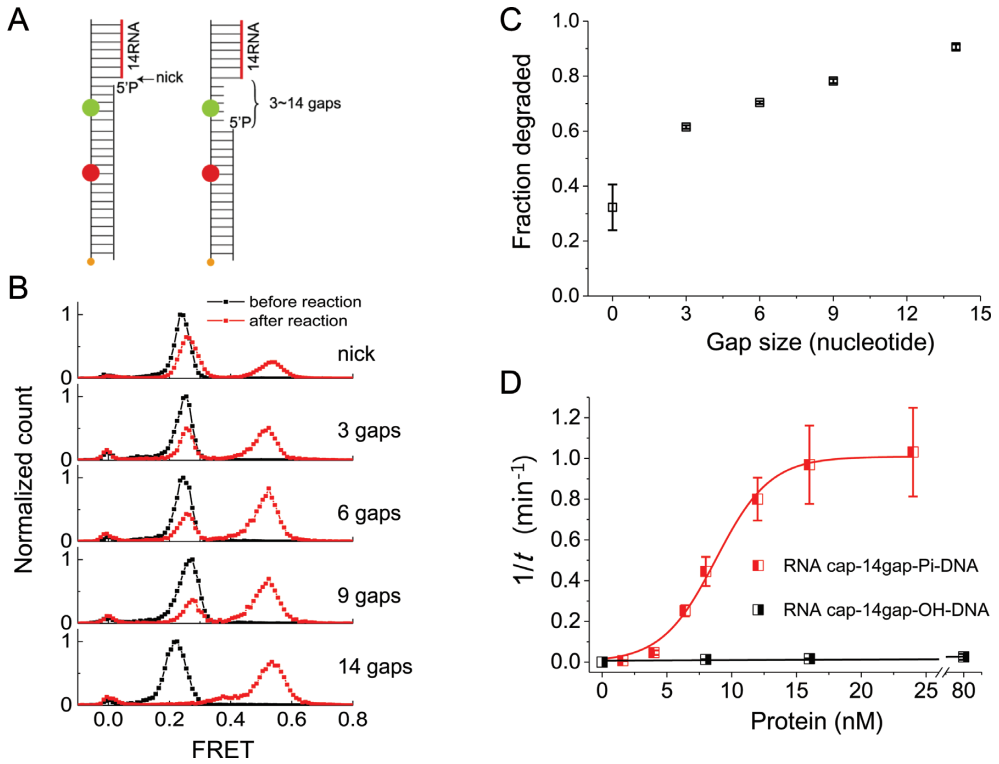

Figure 4. A phosphate at a 5′ recessed DNA functions as an assembly site for trimeric ring formation without passing through the central channel. (**A**) Schematic of hybrid substrates with various gap sizes used to test trimer ring formation. The upstream strand (top) was hybridized with an RNA oligo (red), whereas the downstream strand (bottom) was hybridized with a DNA oligo (black), thus only allowing degradation from the 5′ end of the gap junction. (**B**) Histograms of various gap substrates obtained 2 min after the start of the reaction. (**C**) Fraction degraded vs. gap size, indicating a gap size dependent trimer assembly. (**D**) The inverse of degradation population growth time versus enzyme concentration. The sigmoidal curve suggests allosteric trimer formation for cooperative degradation (see Supplementary Figures S10 and S11). Error bars denote SEM.

firmed that the enzyme indeed could not degrade ssRNA in a DNA/RNA duplex (Supplementary Figure S9).

FRET histograms obtained after a 2-min reaction revealed that the degradation fraction increased upon increasing the ss-gap size between the RNA and DNA oligos (Figure 4B and C). This dependence on gap size in a range between 0 and 14 bp is presumably due to a required footprint (∼13–14 bp) (20) for trimer formation. The degradation of the RNA-blocked substrate ensured its trimeric ring formation around the ssDNA at the ss-/ds-junction if degradation occurs. To further examine assembly kinetics, the protein concentration was increased from 1.6 to 24 nM using the substrate with 14-nt gap, which is longer than the enzyme footprint. The inverse of the degradation-population growth time increased as a function of the protein concentration, suggesting more functional units of the trimer were formed with increasing protein concentrations (Supplementary Figure S10). In addition, the inverse of the time vs. protein concentration plot revealed a sigmoidal curve, demonstrating cooperative degradation and allosteric trimer formation of monomers in solution (Figure 4D, red curve). This data is consistent with a recent study of cooperative binding of λ exonuclease to dsDNA in bulk solution (23).

To further investigate the role of a 5′ phosphate during ring assembly, we removed the 5′ phosphate group and repeated the same assembly experiment. The inverse of the time was dramatically reduced in the absence of the 5′-phosphate (Figure 4D, black curve and Supplementary Figure S11, their distributions). A previous study (21) reported that the R28 residue is responsible for the recognition of the 5′-phosphate at the 5′ end of blunt-ended dsDNA, but how the R28 residue, which is embedded inside the toroidal topology, can recognize a phosphate at the 5′ end of the duplex form is unknown. Our data demonstrated that the 5′-phosphate helps the protein subsequently encircle its strand during the assembly process and this process further places the 5′-end into the active site either via protein binding induced melting or via protein diffusion upon thermal fraying of the terminal bases. However, our current assay could not tell the detailed mechanism such as 'on-site trimer assembly' and 'on-site loading by opening-up of pre-formed trimers in solution'.

DISCUSSION

We developed a single molecule FRET assay that allows us to probe various roles of phosphates, present along linear dsDNA. At the 5′ end of dsDNA, the phosphate contributes to the formation of a catalytically active complex during initiation, consistent with the previous study (21) (Figure 1A). In contrast, hydrolyzing interior phosphates of linear dsDNA facilitates the chemo-mechanical melting at the ss-/ds-junction via successive electrostatic attraction by continuous translocation. Finally, a phosphate at a 5′ recessed duplex DNA facilities the assembly of the trimeric ring, thus

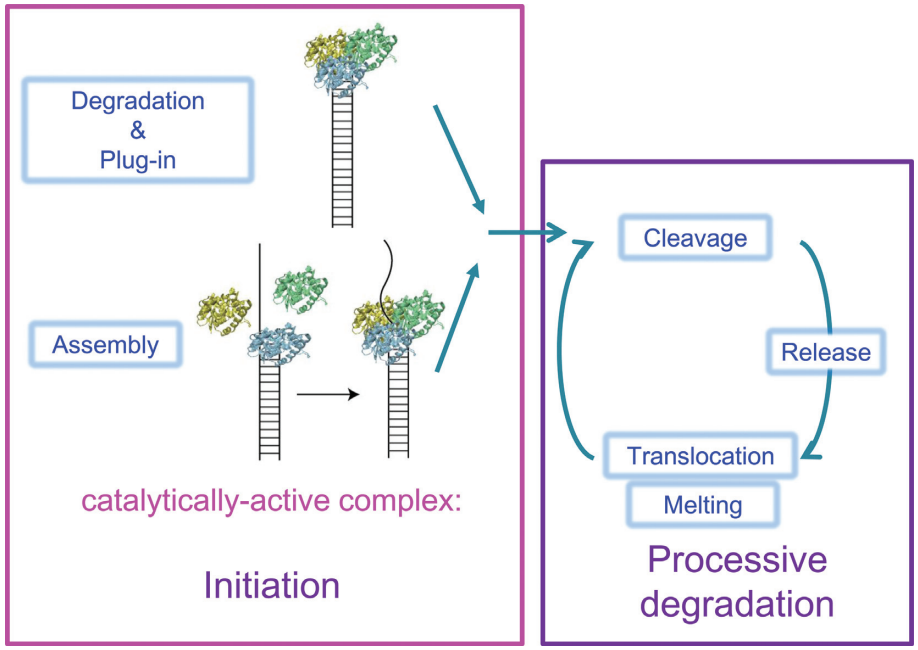

Figure 5. Model of DNA degradation by λ exonuclease. Initiation is achieved by two methods: plug-in at the blunt-end of linear DNA and trimer ring assembly at the single-/double-stranded junction of a partial duplex. The order of processive degradation is cleavage, product release, and translocation by electrostatic attraction with concomitant melting.

allowing degradation to restart or initiate without threading the 3′ ssDNA through the central channel of the enzyme.

Two nucleotides of the 5′ ended strand should be melted before cleavage and inserted into the active site to form the catalytically active complex (Figure 1A). Two types of melting reactions are noted depending on the phase of degradation: cleavage-independent melting during initiation and post-cleavage melting during processive degradation. Cleavage-independent melting is passive as it requires waiting for thermal melting of the fork junction. In contrast, post-cleavage melting via electrostatic attraction is active as the process directly pulls the next bases at the junction. Backtracking events are one method used to pass a nick via passive melting by exposing the ss-/ds-junction to thermal bath at room temperature. Similar mechanistic questions have been debated for other enzymes (6,24–25).

Based on the crystal structural study that suggested that base-pair melting occurs prior to cleavage (19) and our single-molecule study that suggested that the enzyme utilizes two pathways to initiate the reaction depending on the substrate type, we reconstituted the whole reaction cycle with the following order: ***initiation***: engaging or assembly → ***processive degradation***: bond cleavage → product release → electrostatic attraction → concomitant melting of the next base at the junction and 5′ to 3′ translocation by 1-nt along the DNA (Figure 5). Our study offers novel mechanistic insights into the versatile roles of phosphates along the DNA during degradation. The fundamental roles of phosphates as discovered in this single molecule study are potentially common to many DNA and RNA–protein interactions.

SUPPLEMENTARY DATA

Supplementary Data are available at NAR Online.

ACKNOWLEDGEMENT

We thank Suyeon Park and Junhyeok Song for experimental help.

FUNDING

National Research Foundation of Korea (NRF) grants funded by the Korea government [NRF-2012R1A1A1044004, NRF-2013R1A2A2A03067442]; the National R&D Program for Cancer Contol, Ministry of Health & Welfare, Republic of Korea [1320110]; Bio Imaging Research Centre at GIST. Funding for open access charge: Bio Imaging Research Centre at GIST.

Conflict of interest statement. None declared.

REFERENCES

1. Ceska,T.A. and Sayers,J.R. (1998) Structure-specific DNA cleavage by 5 ‘ nucleases. *Trends Biochem. Sci.*, **23**, 331–336.
2. Muyrers,J.P.P., Zhang,Y.M., Buchholz,F. and Stewart,A.F. (2000) RecE/RecT and Red alpha/Red beta initiate double-stranded break repair by specifically interacting with their respective partners. *Genes Dev.*, **14**, 1971–1982.
3. Black,L.W. (1989) DNA packaging in DSDNA bacteriophages. *Annu. Rev. Microbiol.*, **43**, 267–292.
4. Hillyar,C.R.T. (2012) Genetic recombination in bacteriophage lambda. *Biosci. Horiz.*, **5**.
5. Jinek,M., Coyle,S. and Doudna,J. (2011) Coupled 5’ nucleotide recognition and processivity in Xrn1-mediated mRNA decay. *Mol. Cell*, **41**, 600–608.
6. Lee,G., Bratkowski,M.A., Ding,F., Ke,A. and Ha,T. (2012) Elastic coupling between RNA degradation and unwinding by an exoribonuclease. *Science*, **336**, 1726–1729.
7. Myong,S., Bruno,M.M., Pyle,A.M. and Ha,T. (2007) Spring-loaded mechanism of DNA unwinding by hepatitis C virus NS3 helicase. *Science*, **317**, 513–516.

8. Liu,B., Baskin,R.J. and Kowalczykowski,S.C. (2013) DNA unwinding heterogeneity by RecBCD results from static molecules able to equilibrate. *Nature*, **500**, 482–485.
9. Lee,G., Hartung,S., Hopfner,K.P. and Ha,T. (2010) Reversible and controllable nanolocomotion of an RNA-processing machinery. *Nano Lett.*, **10**, 5123–5130.
10. van Oijen,A.M., Blainey,P.C., Crampton,D.J., Richardson,C.C., Ellenberger,T. and Xie,X.S. (2003) Single-molecule kinetics of lambda exonuclease reveal base dependence and dynamic disorder. *Science*, **301**, 1235–1238.
11. Comstock,M.J., Whitley,K.D., Jia,H., Sokoloski,J., Lohman,T.M., Ha,T. and Chemla,Y.R. (2015) Direct observation of structure-function relationship in a nucleic acid -processing enzyme. *Science*, **348**, 352–354.
12. Arslan,S., Khafizov,R., Thomas,C.D., Chemla,Y.R. and Ha,T. (2015) Engineering of a superhelicase through conformational control. *Science*, **348**, 344–347.
13. Hohng,S., Zhou,R.B., Nahas,M.K., Yu,J., Schulten,K., Lilley,D.M.J. and Ha,T.J. (2007) Fluorescence-force spectroscopy maps two-dimensional reaction landscape of the Holliday junction. *Science*, **318**, 279–283.
14. Woodside,M.T., Anthony,P.C., Behnke-Parks,W.M., Larizadeh,K., Herschlag,D. and Block,S.M. (2006) Direct measurement of the full, sequence-dependent folding landscape of a nucleic acid. *Science*, **314**, 1001–1004.
15. Sun,B., Johnson,D.S., Patel,G., Smith,B.Y., Pandey,M., Patel,S.S. and Wang,M.D. (2011) ATP-induced helicase slippage reveals highly coordinated subunits. *Nature*, **478**, 132–135.
16. Perkins,T.T., Dalal,R.V., Mitsis,P.G. and Block,S.M. (2003) Sequence-dependent pausing of single lambda exonuclease molecules. *Science*, **301**, 1914–1918.
17. Aslanidis,C. and De Jong,P.J. (1990) Ligation-independent cloning of PCR products (LIC-PCR). *Nucleic Acids Res.*, **18**, 6069–6074.
18. Lee,G., Yoo,J., Leslie,B.J. and Ha,T. (2011) Single-molecule analysis reveals three phases of DNA degradation by an exonuclease. *Nat. Chem. Biol.*, **7**, 367–374.
19. Zhang,J., McCabe,K.A. and Bell,C.E. (2011) Crystal structures of λ exonuclease in complex with DNA suggest an electrostatic ratchet mechanism for processivity. *Proc. Natl. Acad. Sci. U.S.A.*, **108**, 11872–11877.
20. Mitsis,P.G. and Kwagh,J.G. (1999) Characterization of the interaction of lambda exonuclease with the ends of DNA. *Nucleic Acids Res.*, **27**, 3057–3063.
21. Subramanian,K., Rutvisuttinunt,W., Scott,W. and Myers,R.S. (2003) The enzymatic basis of processivity in lambda exonuclease. *Nucleic Acids Res.*, **31**, 1585–1596.
22. Sriprakash,K.S., Lundh,N., Mooonhuh,M. and Radding,C.M. (1975) Specificity of lambda-exonuclease interactions with single-stranded-DNA. *J. Biol. Chem.*, **250**, 5438–5445.
23. Pan,X., Smith,C.E., Zhang,J., McCabe,K.A., Fu,J. and Bell,C.E. (2015) A structure-activity analysis for probing the mechanism of processive double-stranded DNA digestion by λ exonuclease trimers. *Biochemistry*, **54**, 6139–6148.
24. Kerssemakers,J.W.J., Munteanu,E.L., Laan,L., Noetzel,T.L., Janson,M.E. and Dogterom,M. (2006) Assembly dynamics of microtubules at molecular resolution. *Nature*, **442**, 709–712.
25. McKinney,S.A., Joo,C. and Ha,T. (2006) Analysis of single-molecule FRET trajectories using hidden Markov modeling. *Biophys. J.*, **91**, 1941–1951.